Atmospheric
Chemistry
and Physics
Discussions

Open Access

EGU

1 **Measurement report: Characteristics and sources of non-methane**

2 **VOCs and their roles in SOA formation during autumn in a central**

3 **Chinese city**

4

5 Haixu Zhang[1,2], Chunrong Chen[1], Weijia Yan[1], Nana Wu[1], Yu Bo[3], Qiang Zhang[1], and

6 Kebin He[2,4]

7 [1] Ministry of Education Key Laboratory for Earth System Modelling, Department of Earth System

8 Science, Tsinghua University, Beijing 100084, China

9 [2] State Key Joint Laboratory of Environment Simulation and Pollution Control, School of

10 Environment, Tsinghua University, Beijing 100084, China

11 [3] RCE-TEA, Institute of Atmospheric Physics, Chinese Academy of Science, Beijing 100029, China

12 [4] State Environmental Protection Key Laboratory of Sources and Control of Air Pollution Complex,

13 Tsinghua University, Beijing 100084, China

14

15 Correspondence: Haixu Zhang (zhanghaixu@tsinghua.edu.cn) and Yu Bo (boyu@mail.iap.ac.cn)

16

Abstract

17

18   Volatile organic compounds (VOCs) are essential in secondary organic aerosol

19   (SOA) formation due to their dual roles as precursors and oxidant producers. In this

20   work, the VOC species in Xinxiang, a mid-sized city located in Henan Province in

21   central China, were measured and analysed from November 5th to December 3rd, 2018.

22   Based on online monitoring with proton transfer reaction-mass spectrometry (PTR-MS)

23   and canister grab samples, 53 VOC species are obviously detected, and the most

24   abundant categories are oxygenated VOCs (OVOCs) and benzenoids. Compared with

25   field measurements in other regions, the mixing ratios of BTEX (benzene, toluene,

26   ethylbenzene, and xylene), acetaldehyde, and C3 carbonyls are at high levels, indicating

27   intensive anthropogenic emissions in Xinxiang. According to the positive matrix

28   factorization (PMF) model, benzenoids are mainly emitted from solvent evaporation

29   (~47%), residential heating (~19%), industrial emission (~16%), and vehicle exhaust

30   (~10%), while the contributions from biogenic and secondary sources as well as thermal

31   power generation are minor. However, the emissions of total OVOCs from the six

32   resolved sources are similar. The potential source contribution function (PSCF) and

33   concentration weighted trajectory (CWT) results show that the transport contribution

34   for VOCs is not intensive, but the cities within Henan Province or in the neighbouring

35   provinces may influence the mixing ratios to some extent. The roles of benzenoids and

36   OVOCs in SOA formation are investigated by estimating the mass of oxidation

37   products and rates of OH radical production. Among the observed VOCs, toluene has

38   the largest SOA formation potential (SOAFP), while its weight in SOA formation

39   declines with the aggravation of pollution. On the other hand, the SOA concentration

40   shows a good relationship with OH exposure, which highlights the importance of the

41   atmospheric oxidation capacity, especially in polluted periods. Formaldehyde is the

42   strongest radical contributor, and the contribution of acetaldehyde is also significant in

43   this study. Furthermore, solvent evaporation, industrial emissions, and vehicle exhaust

44   are estimated as the top three anthropogenic contributors with the highest SOAFP and

45   radical contribution rate.

46

1. Introduction

The haze problem in China has attracted much attention in recent decades. Many observation studies have shown that secondary organic aerosol (SOA) comprises a major fraction of the fine particle mass, and some recent studies highlight the driving force of SOA in extremely severe pollution episodes (Crounse et al., 2013; Guo et al., 2014; Huang et al., 2014). The level of SOA is primarily determined by both the concentrations of gaseous precursors and atmospheric oxidizing capacity (Rao et al., 2016). Therefore, volatile organic compounds (VOCs) are critical in SOA formation because of their roles as precursors and active participants in the cycling of free radicals (Atkinson et al., 2008; Kroll and Seinfeld, 2008; Lelieveld et al., 2008). Among hundreds of VOC species, aromatic hydrocarbons constitute an important fraction (~20–30%) of the urban atmosphere and have been suggested to be important SOA precursors in many studies (Calvert, 2002; Ding et al., 2014; Yuan et al., 2013; Wu and Xie, 2018). Oxygenated volatile organic compounds (OVOCs) are also an important category of species because they are not only essential members of oxidation processes but also the most important radical sources in polluted urban environments (Shao et al., 2011; Kristensson et al., 2004; Emmerson et al., 2005; Edwards et al., 2014).

To aid in SOA estimation, many laboratory studies have investigated the SOA yield of individual precursors. Accordingly, the ambient SOA yield cannot be represented by a unique value because it is dependent on the organic aerosol mass concentration, NOx concentration and temperature (Odum et al., 1996; Rollins et al., 2012; Sarrafzadeh et al., 2016). The two-product model considering the above influencing factors is a widely used SOA yield model in three-dimensional chemical transport models (Appel et al., 2008; Tsimpidi et al., 2011; Li et al., 2015), but it is scarcely applied to SOA estimation in field studies to our knowledge. Regarding photooxidants, numerous measurements have been conducted focusing on the performance of OVOCs at different stages of pollution and their potential sources (Duan et al., 2012; Yang et al., 2017; Li et al., 2010; Liu et al., 2012), and only a few studies have conducted quantitative analyses on radical production rates based on field

76 observations in China by utilizing a tropospheric ultraviolet and visible (TUV, version

77 5.0; http://cprm.acd.ucar.edu/Models/TUV/) radiation model (Rao et al., 2016; Wang

78 et al., 2017).

79 Vehicle exhaust emissions, industry emissions, fossil fuel volatilization, the use of

80 chemical reagents, and biomass combustion are important sources of atmospheric

81 VOCs, but there are some differences in different regions (Qi et al., 2014; Yang et al.,

82 2013; Li et al., 2019a; Liu et al., 2017; Zheng et al., 2018). In addition, the source

83 apportionment of OVOC sources, especially carbonyls, still has many uncertainties due

84 to the complex sources and sinks (Huang et al., 2019; Chen et al., 2014). The sources

85 show different chemical reactivities because of the VOC compositions. Hence, an

86 inventory-based SOA formation potential (SOAFP) list in China has been made to

87 identify the major species and sources contributing to SOA (Wu and Xie, 2018). In

88 some field studies, the SOAFP calculation is also applied to reveal the atmospheric

89 characteristics and the critical components for SOA increase, but few studies compare

90 the SOAFP among the resolved sources (Zhang et al., 2017; Zhang et al., 2018; Han et

91 al., 2020).

92 Xinxiang, a central city in China, has been within the most polluted region in

93 recent years. During the autumn of 2018, we conducted a field study focusing on the

94 characteristics of VOCs at an urban site in Xinxiang for the first time. In this work, the

95 mixing ratios, temporal variations, and diurnal patterns of the VOCs are shown and

96 compared with those at other sites. Source apportionment and regional contributions

97 are investigated based on the PMF model, as well as PSCF and CWT analyses. The

98 roles of benzenoids and OVOCs in SOA formation are investigated by estimating the

99 mass of oxidation products and rates of OH radical production, respectively, with

100 parameters (such as SOA yields and photolysis rates) based on real-time data. Finally,

101 the information about SOAFP as well as the radical producing capacity are first

102 assigned to the resolved source.

103 **2. Experiment**

104 **2.1 Sampling site and measurements**

105   The measurements were performed in a mobile laboratory located in a square of

106   the Party School in Xinxiang. The sampling site was tens of metres away from a

107   national air quality monitoring site (35.3N, 113.9E) in the urban district (Hongqi

108   District). The surroundings were residential areas and colleges, except for a few

109   pharmaceutical factories 2 km to the west.

110   The VOC concentrations were observed by utilizing quadrupole proton transfer

111   reaction-mass spectrometry (PTR-QMS 500, Ionicon Analytik, Austria). The

112   observation principle and the deployment of PTR-MS have been described in many

113   previous studies (Lindinger et al., 1998; Yuan et al., 2013; Li et al., 2019b). Briefly,

114   only the species with a proton affinity greater than that of H_2O (691 kJ mol^{-1}) can be

115   detected. In this work, the PTR-MS was operated at a standard condition: the pressure

116   of the drift tube was held at 2.2 mbar, and the temperatures of the inlet line and the drift

117   tube were both kept at 60 °C, with the reduced electric field parameter (E/N, where E

118   is the electric field and N is the gas number density) maintained at 135 Td. Air samples

119   were drawn through a Teflon line with an inner diameter of 0.125 cm. The VOC

120   measurements were performed in full-scan mode, browsing a large range of masses

121   (m/z 21.0—200.0), with a time resolution of ~10 s. In all, 44 mass peaks were involved

122   in this study, and the attribution of each peak to specific VOC species is summarized

123   in Table S1 of the supplement. The VOCs analysed as focus or tracers are 1. m/z 31

124   (formaldehyde); 2. m/z 33 (methanol); 3. m/z 42 (acetonitrile); 4. m/z 45 (acetaldehyde);

125   5. m/z 47 (formic acid and ethanol); 6. m/z 59 (acetone); 7. m/z 69 (isoprene); 8. m/z

126   71 (methyl vinyl ketone and methacrolein, MVK+MACR); 9. m/z 79 (benzene); 10.

127   m/z 93 (toluene); 11. m/z 105 (styrene); and 12. m/z 107 (C8 aromatics, including

128   ethylbenzene and xylenes). The PTR-MS was calibrated regularly with a dynamic

129   calibrator (Model 146i, Thermo Scientific, USA) using two standard gas cylinders

130   containing formaldehyde with a mixing ratio of 10 ppm and 17 other VOCs with a

131   mixing ratio of 1 ppm of each species. The instrument background calibration was

132   performed by installing a charcoal cartridge (Supelco, USA) upstream of the PTR-MS

133   inlet. PTR-MS Viewer software (Version 3.1, Ionicon Analytik, Austria) was used to

134   calibrate the transmission curve and process the observed data. More information on

135   the calibration process and the list of the 17 standard gases are shown in Text S1 of the

136   supplement.

137   In addition, 27 grab samples were collected using 3.2 L SUMMA canisters (Entech

138   Instrument, USA) with a sample duration of 1 h in the daytime, and the specific

139   sampling time is listed in Table S2. Before sampling, the canisters were precleaned with

140   high-purity nitrogen and pressurized to 50 psi, and one of them was then filled with

141   high-purity nitrogen as a blank sample. The chemical analysis was accomplished within

142   2 weeks after sampling, based on Compendium Method TO-15 (EPA, 1999). Briefly,

143   in this work, the air samples in the canisters were initially concentrated at -160 ℃ using

144   liquid nitrogen in a cryogenic preconcentrator (7100A, Entech, USA) to remove CO_2

145   and H_2O. Then, the samples were thermally desorbed at 120 ℃ and transported into a

146   GC-MS system (Model 7890A-5975C, Agilent Technologies, USA) with a DB-624

147   column (60 m×25 mm inner diameter with 1.4 μm film thickness) for analysis. The

148   standard gas of PAMS and TO 15 (1 ppm; Spectra Gases, USA) was used to construct

149   the calibration curves. In total, VOC species were effectively observed including 12

150   alkanes, 12 halohydrocarbons, and 14 aromatic hydrocarbons. No alkenes, alkynes or

151   C1-C2 alkanes were detected under the existing conditions.

152   The mass concentration of organic aerosol (OA) of NR-PM_1 was measured by an

153   Aerosol Chemical Speciation Monitor (ACSM, Aerodyne, USA), with a time resolution

154   of 15 min. The details of instrument operation and data analysis have been described in

155   previous studies (Ng et al., 2011; Li et al., 2018). The oxygenated OA (OOA) was

156   determined by utilizing the PMF model (Li et al., 2018), and the resolved results are

157   shown in Text S2 and Figs. S1-2. In this study, OOA is approximately treated as SOA.

158   The SO_2, CO, NO_x, and O_3 concentrations were measured by corresponding gas

159   analysers (Model 43i-TLE, 48i-TLE, 17i, and 49i, Thermo Scientific, USA). The $PM_{2.5}$

160   mass concentration was measured online by utilizing a heated tapered elemental

161   oscillating microbalance (TEOM series 1405, Thermo Scientific, USA), and the

162   meteorological conditions, including temperature, RH, pressure, wind speed, and wind

163   direction, were continuously reported by a portable weather station (WXT536, Vaisala,

164   Finland). In addition, the heights of the planetary boundary layer (PBL) were provided

165   by the local environmental monitoring station from their lidar station.

166   **2.2   Source apportionment**

167   The US EPA Positive Matrix Factorization (PMF) receptor model (version 5.0,

168   Sonoma Technology, Inc. USA), based on the multi-linear engine (ME-2) approach,

169   was used for source apportionment. The relevant parameters and calculation principles

170   have been described explicitly in previous studies (Norris G., 2014; Sarkar et al., 2017).

171   In the current work, 610 hourly averaged samples were involved, with 44 species

172   including 41 ion peaks from PTR-MS as well as CO, SO_2, and NO_X. The corresponding

173   uncertainties were calculated from the method detection limit (MDL) and the

174   determination error fraction, which is recommended by the user guide (Norris G., 2014).

175   Detailed information about the operation principle and the input data is described in

176   Text S3 and Table S1. The PMF was performed with 20 base runs, and the result with

177   the lowest Q (robust) value was chosen. To determine the optimum solution, PMF

178   model runs with 2 to 10 factor numbers were carried out.

179   **2.3 Trajectory analysis**

180   In this study, 48 h backward trajectory analysis with 1 h intervals (starting from

181   00:00 to 23:00 local time, LT) was performed each day at a height of 500 m above

182   ground level with the Hybrid Single-Particle Lagrangian Integrated Trajectory

183   (HYSPLIT) model (http://www.noaa.gov, last access: 10 February 2020). The results

184   were saved as endpoint files and further processed for trajectory clustering and statistics

185   using   MeteoInfo   software   plugged   in   with   TrajStat

186   (http://www.meteothinker.com/downloads/index.html, last access: 10 February 2020).

187   The spatial distributions of the identified sources were thereby analysed with PSCF and

188   CWT, which indicated the proportion of the source contribution in a given grid and the

189   concentration levels of the trajectories, respectively. In this study, the domain area was

190   in the range of 32-42ºN, 100-120ºE with a resolution of 0.5º×0.5º. More details on the

191   description can be obtained in Text S4.

192 **2.4 SOA production estimation**

193   In this study, a parametrization method was used to estimate the SOA formation

194 potential (SOAFP) as well as the real-time SOA production, and the formula is listed

195 as follows:

$$SOAFP_i = VOC_i \times Y_i \tag{1}$$

$$SOA_i = VOC_{i,consumed} \times Y_i \tag{2}$$

198   where Y_i is the SOA yield of VOC_i, which can be initially estimated according to

199 the OA concentrations and VOC/NOx conditions using two-product models summed

200 up by previous chamber studies (Lim and Ziemann, 2009; Ng et al., 2007). For species

201 lacking yield curves, the fractional aerosol coefficient (FAC) values proposed by

202 Grosjean and Seinfeld (1989) were used. Furthermore, the yields were corrected for

203 vapor wall losses according to a recent study (Zhang et al., 2014). The SOA yields

204 estimated in this study and the corresponding references are shown in the supplement

205 as Table S3. VOC_i and $VOC_{i,\ consumed}$ represent the initial emission and the real amount

206 of VOC_i oxidized by the OH radical, which can be calculated with the photochemical

207 age (de Gouw et al., 2005; Warneke et al., 2007):

$$VOC_i = VOC_{i,t} \times \exp(k_i[OH]\Delta t) \tag{3}$$

$$VOC_{i,consumed} = VOC_i - VOC_{i,t} \tag{4}$$

210   where $[OH]\Delta t$ represents the OH exposure, which can be estimated based on the

211 ratio of (MACR+MVK)/isoprene according to previous studies (Santos et al., 2018;

212 Apel et al., 2002; Stroud et al., 2001; de Gouw et al., 2005). Accordingly, the OH-

213 driven isoprene oxidation and the sequential reaction model can be described as:
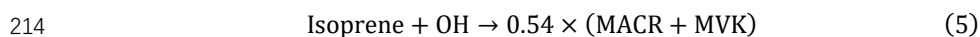
$$Isoprene + OH \rightarrow 0.54 \times (MACR + MVK) \tag{5}$$

$$k_I = 1 \times 10^{-10} \text{ cm}^3 \text{ molecule}^{-1} \text{ s}^{-1}$$

$$(MACR + MVK) + OH \rightarrow Product \tag{6}$$

217   The derived expression can be used to estimate the photochemical age, which is

218 shown as follows:

$$\frac{[MACR + MVK]}{[Isoprene]} = \frac{0.54k_1}{(k_2 - k_1)}\left(1 - e^{(k_1 - k_2)[OH]\Delta t}\right) \tag{7}$$

220

Atmospheric
Chemistry
and Physics
Discussions

2.5 Radical contribution quantification

Hydroxyl radicals (OH) are the most important oxidants in the troposphere atmosphere, which mainly originate from the photolysis of O_3, OVOCs, and HONO (Crutzen et al., 1991). Except for in the morning, carbonyl compounds and O_3 are major precursors of OH. In this study, the production rates of OH from O_3 and typical carbonyls (formaldehyde, acetaldehyde, and acetone) were calculated using the following formulas:

$$P\left(OH_{O_3}\right) = \frac{2J_{O_3}[O_3]k_1[H_2O]}{k_1[H_2O] + k_2[O_2] + k_3[N_2]} \quad (8)$$

$$P\left(OH_{Carbonyl_i}\right) = 2 \times J_{i,l}[Carbonyl_i] \quad (9)$$

where J_{O_3} and $J_{i,1}$ represent the photolysis rate constants of O_3 and carbonyl compounds, respectively, which are obtained from the TUV model. The model calculates the solar shortwave radiation between 120 and 735 nm with most parameters set at default values, except for the aerosol optical depth (AOD). The AOD is set as 0.7 for non-haze days and 1.5 for haze days, as in previous studies in Beijing (Liang et al., 2013; Rao et al., 2016). In formula (8), k_1, k_2, and k_3 represent the reaction rate constants of O (1D) with H_2O, O_2, and N_2, respectively, which are obtained from the National Institute of Standard and Technology (NIST) Chemical Kinetics Database (https://kinetics.nist.gov/kinetics/, Standard Reference Database 17, Version 7.0). It needs to be noted that in Eq. (9), all the RO_X produced from the photolysis reaction can be assumed to be completely converted into HO, which is the case in most periods during the daytime. Therefore, the results show the upper limit of the carbonyl contribution (Wu et al., 2017; Zheng et al., 2013). Furthermore, the yield of radicals (Y) of a carbonyl from the main reactions in the daytime can be calculated as:

$$Y = \frac{2 \sum_{i=1}^{n} J_{i,1}[OVOC]_i}{\sum_{i=1}^{n}(J_{i,1} + J_{i,2} + \cdots\cdots + J_{i,m})[OVOC]_i + \sum_{i=1}^{n} k_{i,OH}[OH][OVOC]_i} \quad (10)$$

where $J_{i,2-m}$ represents the photolysis rates without the formation of OH radicals, which is also estimated with the TUV model. In addition, $k_{i,OH}$ is the rate constant for the reaction of carbonyl with OH radicals. [OH] is set as 0.62×10^6 molecules cm^{-3} on

Atmospheric
Chemistry
and Physics

Open Access

EGU

Discussions

248   clear days and 0.46×10^6 molecules cm^{-3} on hazy days, calculated using the following

249   equation, based on a parameterization method (Ehhalt and Rohrer, 2000).

250    $$[OH] = 4.1 \times 10^9 \times (J_{O1D})^{0.83} \times (J_{NO2})^{0.19} \times \frac{140 \times [NO_2] + 1}{0.41 \times [NO_2]^2 + 1.7 \times [NO_2] + 1} \quad (11)$$

251   Here, J_{O1D} and J_{NO2} are the estimated photolysis frequencies (s^{-1}) of O$_3$ and NO$_2$

252   with the TUV model, respectively. [NO$_2$] is the measured NO$_2$ concentration (ppbv,

253   parts per billion by volume).

254   **3.   Results and discussion**

255   **3.1   Mixing ratio of VOCs**

256   As previously described, PTR-MS is highly efficient for detecting OVOCs and

257   benzenoids but useless for detecting alkanes because of the limitation of the proton

258   affinities. Therefore, the composition of VOC species is initially summed up by

259   integrating the observation data from PTR-MS and canister sampling. The concordance

260   of the observed data from the two measurements is checked using the species that can

261   be detected from both methods, and the results show a good relationship between the

262   two methods for benzene (r=0.90). On average, the observed benzene concentration

263   from PTR-MS is 12% higher than those from canister sampling. Figure 1 shows the

264   average mixing ratios of different VOC categories during the sampling period,

265   including alkanes (>C6), benzenoids, alkenes, halogenated hydrocarbons, nitrogen-

266   containing compounds (N-VOCs), sulfur-containing compounds (S-VOCs), and

267   OVOCs. Accordingly, the mixing ratio of OVOCs is more than 5-fold that of the others.

268   Among the major radical contributors—carbonyl compounds—acetaldehyde has the

269   highest average concentration, followed by a mixture of acetone and propionaldehyde,

270   as well as formaldehyde. In addition, alcohols such as methanol and ethanol exhibit

271   high levels, which might be largely due to the combustion process (Sahu and Saxena,

272   2015; Holzinger et al., 2005; Brito et al., 2015). Benzenoids are the second most

273   abundant category, and the major components are benzene, toluene, and C8 aromatics.

274   Under the current instrument configuration, short-chain alkanes and unsaturated

275   hydrocarbons cannot be detected effectively. The alkanes with more than two carbon

276   atoms have an average mixing ratio of 1.47 ppbv and are mostly cycloalkanes, heptane,

277 and octane. The alkenes contain isoprene, pinenes, and styrene, with a total

278 concentration of 1.61 ppbv. In addition, the observed N-VOCs and halohydrocarbons

279 have mixing ratios of 2.55 and 2.64 ppbv, respectively. Finally, only CS_2 and dimethyl

280 sulfide can be detected for the S-VOC category, with a total concentration of 0.62 ppbv.

281   Figure 2 shows a comparison between the mixing ratios of carbonyls and

282 benzenoids measured in Xinxiang, with the observed results reported elsewhere.

283 Overall, the average VOC concentrations are among the highest levels worldwide.

284 Formaldehyde has been regarded as the largest radical contributor in winter, while the

285 average concentrations in Xinxiang on both hazy days and non-hazy days are lower

286 than those of most recent studies in China (Qian et al., 2019; Sheng et al., 2018; Yang

287 et al., 2019; Su et al., 2019). In contrast, the average concentrations of acetaldehyde

288 and C3 carbonyls on both hazy and non-hazy days are commonly higher than those in

289 previous studies. The concentrations of benzenoids are generally above the worldwide

290 level except for some severe pollution periods in China and India (Sahu et al., 2016;

291 Sheng et al., 2018; Liu et al., 2015; Sinha et al., 2014). In autumn and wintertime, the

292 above carbonyl compounds and benzenoids are mainly from anthropogenic emissions

293 (Qian et al., 2019; Yang et al., 2019; Barletta et al., 2005; Zhang et al., 2015). Therefore,

294 poor diffusion conditions and intensive emissions are the major reasons for the high

295 concentrations of VOCs on hazy days. It is obvious that the formaldehyde, toluene, and

296 C8 aromatics show slighter enhancements from non-hazy days to hazy days, probably

297 because of the fast consumption owing to their high photolysis and photochemical rates.

298 **3.2 Meteorological conditions and diurnal variations**

299   It has been shown that pollutant dispersion is primarily related to wind direction

300 and speed, while atmospheric chemical reactions can be influenced by temperature and

301 humidity (Greene et al., 1999). In Fig. 3, the hourly averaged data of the meteorological

302 parameters and the concentration of pollutants including OVOCs, benzenoids, and

303 some inorganic gases are displayed. During the investigated period, the temperature

304 and RH show opposite diurnal fluctuations, and both show significant changes after

305 entering the second half of November. In particular, RH remained high on 12-14

306   November and 1-3 December, which might provide a preferable environment for

307   sulfate and OA increases (Jathar et al., 2016; Sun et al., 2013; Tang et al., 2018). It is

308   evident that the variation trends of the pollutant concentrations are highly ascribed to

309   atmospheric diffusion characterized by wind speed and PBL height. The first peak of

310   benzenoids, on 9-10 November, appears after a valley of PBL and dozens of hours of

311   low wind speed. During 12-15 November, the high concentration levels of both OVOCs

312   and benzenoids occur with sustained low wind speed (< 2 m/s), and this state is

313   dispersed with the increased wind speed after 12:00 on 15 November, along with a

314   significant increase in PBL height. In the last period of haze (especially after 23

315   November), the VOC concentrations fluctuate at a high level, and the wind direction is

316   more concentrated in the northeast at speeds of less than 3 m/s. Due to the

317   implementation of motor vehicle restrictions, the benzenoid concentration during this

318   period is lower than that on the last hazy days. An investigation in northern China

319   proposed that high pressure followed by a low-pressure system and front zone is in

320   accordance with the increasing phase, maximum values, and decreasing phase of

321   pollution (Chen et al., 2008), and this pressure pattern can be clearly observed and used

322   to explain the accumulation process on 7-9, 16-20, and 24-26 November. The

323   meteorological conditions on 1-3 December accord with both poor diffusion conditions

324   (shallow PBL) and accumulation pressure patterns; therefore, pollutants such as

325   OVOCs, benzenoids and CO show an increasing tendency afterwards. It should be

326   noted that the variation trend of SO_2 does not agree with the others, especially on 1-3

327   December. This phenomenon shows that the major source of SO_2 is quite different,

328   which might be due to long-distance transportation.

329   Prior to the investigation into the variation characteristics of typical carbonyls and

330   benzenoids, daily changes in temperature, RH, wind speed, and air pressure are

331   demonstrated in Fig. S3 to distinguish the influences of meteorological factors. In

332   addition, the diurnal changes in some inorganic gases (NOx, SO_2, and CO) are

333   investigated as tracers of typical sources, as shown in Fig. S4. The detailed analysis

334   referring to the diurnal variation law of meteorology and tracers is described in Text S5.

335   Briefly, atmospheric pollutants tend to accumulate in the morning and disperse in the

336   afternoon along with changes in atmospheric stability. NO_X and CO show the bimodal

337   features of vehicle emissions, and SO_2 represents the regional influence of coal

338   combustion. According to Fig. 4, the concentrations of all the carbonyl species begin

339   to climb after sunrise and reach high concentrations around noon, which might partly

340   result from secondary photochemical production. Meanwhile, industrial activities are

341   completely resumed during the daytime, contributing to the above concentration pattern.

342   The right Y-axis in Fig. 4 represents the ratio of the concentration to the value at 0:00

343   LT. Comparatively, the increase ratio of the C3 carbonyl mixture is the highest,

344   followed by those of acetaldehyde and formaldehyde, which has an inverse correlation

345   to the photolysis rates among formaldehyde, acetaldehyde, and acetone. Therefore,

346   photochemical consumption plays an essential role in carbonyl compound behaviour in

347   the atmosphere, and the mixture of C3 carbonyls may be dominated by acetone. The

348   correlation coefficient between benzene and CO is 0.92, and their diurnal variation is

349   quite similar. The reaction activity of toluene in photochemistry is strong; therefore, the

350   concentration after 12:00 LT decreases sharply. Figure 4 (f) indicates that C8 aromatics

351   are mainly emitted from solvent usage, and the temperature influence on the

352   evaporation rate can offset the daytime "valley" caused by meteorological conditions

353   in the afternoon.

354   **3.3 Source apportionment of VOCs**

355   Figure 5 shows the correlation between the estimated total VOC concentrations

356   and the measured total VOC concentrations with the coefficient r=0.96, indicating that

357   the source apportionment result fits well with the measured data. The profiles of the

358   sources resolved by the PMF model are shown in Fig. S7, including biogenic and

359   secondary sources, solvent evaporation, residential heating, thermal power generation,

360   vehicle exhaust, and industrial emissions. Details of the source identification are

361   described in Text S6 on the basis of the corresponding tracers and daily variation

362   (shown in Fig. S8). Generally, benzenoids are closely related to coating, solvent usage,

363   industrial processes, and energy structure; therefore, it is difficult to compare the

364 contributions among different seasons and cities in the world (Hui et al., 2018; An et

365 al., 2012). In this study, solvent evaporation is the largest contributor, with a fraction

366 of 47% (shown in Fig. 6 (a)), followed by residential heating (19%) and industrial

367 emission (16%), and this situation occurs because the sampling site is located in a

368 district with industrial zones and restricted traffic during the sampling time.

369   Anthropogenic emissions are found to be the largest contributor of OVOCs

370 (specifically carbonyl compounds) in the current study, which aligns with the previous

371 conclusions about winter (Qian et al., 2019; Chen et al., 2014). Figure 6 (b) shows the

372 distribution of all OVOC emissions from the six sources, and the proportions are close.

373 For individual species, 64% of formaldehyde, the most reactive species for radical

374 production, is contributed by primary anthropogenic emissions, including thermal

375 power plants (19%), industrial emissions (16%), solvent evaporation (11%), and other

376 sources. The main sources of acetaldehyde and C3 carbonyls have been reported as

377 vehicle exhaust, industrial emissions and solvent usage (Qian et al., 2019; Singh et al.,

378 1994), and industrial emission is found to be the largest contributor in this study.

379 **3.4 Regional contribution**

380   In addition to the impact of local emissions, regional transport is considered in this

381 study. As shown in Fig. 7, four clusters exist during the sampling time. In total, the

382 dominant air masses are from the southwest direction, including long-distance transport

383 mainly from western Inner Mongolia (20.0%) and medium-distance transport from

384 Shaanxi and Shanxi Provinces (34.2%). The proportion clusters from the northeast

385 (passing through the BTH region) and southeast (from southern Henan province and

386 some areas in Hubei, Anhui, and Jiangsu province) are 21.5% and 24.3%, respectively,

387 with a relatively shorter distance. According to the PSCF and CWT results in Fig. 8 and

388 Fig. 9, the VOC concentrations are dominated by local emissions and can be influenced

389 by cities within Henan Province or in neighbouring provinces. As biogenic emissions

390 are extremely low in northern China in autumn and BVOCs generally actively react

391 within a few hours, Fig. 8 (a) and Fig. 9 (a) represent the spatial origins of the secondary

392 products. The intensity of this source has a relatively high value in northern Shanxi, as

393 well as at the junction of Hebei and Shandong Provinces, which might be influenced

394 by the oxidation of VOCs from other sources. According to Fig. 8 (b) and Fig. 9 (b),

395 hot spots of solvent evaporation are found to the west of Xinxiang. Intensive residential

396 heating emissions (shown in Fig. 8 (c) and Fig. 9 (c)) are also found to the west of

397 Xinxiang, covering the border cities in Henan and Shanxi, which might be due to the

398 high coal production and residents' living habits. Another coal combustion-related

399 source, thermal power generation, has relatively high PSCF and CWT values around

400 the sampling site, with some hot spots observed in the southern region. In Fig. 8 (e) and

401 Fig. 9 (e), the contribution potential of vehicle exhaust is slightly higher from the

402 northwest and source directions. The industrial emission sources are obviously

403 observed around the sampling site with some hot spots except for to the west, which

404 coincides with the real situation, where many plants are located in the remote districts

405 around the urban area.

3.5 Potential roles of VOCs in SOA formation

407 The ratio of VOCs/NOx (ppbC/ppbv) is calculated with the species contributing

408 to SOA formation, and the value is generally below 5 during the investigated period,

409 indicating high NO_X conditions. Based on the estimated yields of the VOCs shown in

410 Table S3, the SOAFPs are calculated and compared in Fig. 10. It should be noted that

411 the yields of mixtures of isomers are estimated based on the yields of individual species

412 and their weighted concentrations (estimated from canister sampling results).

413 Accordingly, aromatics have the largest SOAFP, with contributions of 66%, 7.2%, and

414 4.5% from toluene, benzene, and C8 aromatics, respectively. The estimated SOAFP

415 percentage of alkanes is low in the current study (~2%). Although short chain alkanes,

416 especially species with fewer than 2 carbon atoms, are not detected in this study; this is

417 not the reason for the low contribution proportion because many previous studies have

418 shown that the yields of alkanes (<C7) are close to zero (Grosjean and Seinfeld, 1989;

419 Gao et al., 2019). Compared to a recent study in a nearby city, Zhengzhou, the observed

420 species of alkanes (>C2) are similar and are mainly emitted from petrochemical sources

421 and oil gas evaporation. To our knowledge, these kinds of sources are not intensive in

422   Xinxiang. Long-chain alkanes (>C12) are intermediate volatile organic compounds

423   (IVOCs) that are of great significance in SOA formation, but they cannot be observed

424   using the current method, which would be the main reason for the underestimation of

425   alkane contributions. The SOAFP contribution of OVOCs in this study (2%) is close to

426   the inventory-based SOAP estimation in the Beijing-Tianjin-Hebei region (1.9%) (Wu

427   and Xie, 2018), which is dominated by some long-chain alcohols and phenols.

428   Based on ACSM analysis, OOA (approximately treated as SOA in this study)

429   accounts for 63±10% of OA during the sampling campaign (shown in Fig. S1). As

430   previous studies described, SOA can be formed via gas-phase oxidation of POA and

431   VOCs, as well as some heterogeneous reactions on aerosol surfaces (Xing et al., 2019).

432   To investigate the proportion of SOA generated from VOC photooxidation in gas

433   phases along with the pollution process, real-time consumption and SOA production of

434   benzene, toluene, and C8 aromatics are calculated based on Eqs. (2)-(7). As shown in

435   Fig. 11, the weights of the benzenoids in SOA formation decline dramatically as the

436   OOA concentration increases from 2 to 5 $\mu g\ m^{-3}$, and the proportions of toluene, C8

437   aromatics, and benzene are approximately 1%, 0.5%, and 0.1%, respectively, with high

438   OOA concentrations. Considering that benzenoids are the precursors with the largest

439   SOAFP, it can be concluded that the direct oxidation of VOCs significantly contributes

440   to SOA accumulation at the initial pollution, but the weight declines with the

441   aggravation of haze.

442   Figure S9 shows the correlation curve of OH exposure versus OA concentration

443   with a correlation coefficient (r=0.65), indicating the identity of the atmospheric

444   oxidation capacity with SOA increase. In Table 1, the modelled average OH

445   concentrations, OH production rates of O_3 and typical carbonyls, and the radical yields

446   of carbonyl compounds on both non-hazy days and hazy days are listed. The estimated

447   OH concentration is close to that of a previous study in Beijing (0.99×10^6 molec cm^{-3}

448   on non-hazy days and 0.34×10^6 molec cm^{-3} on hazy days (Rao et al., 2016)), while the

449   difference in this study is smaller, which might be because of the larger accumulation

450   of photolysis precursors on hazy days in Xinxiang. Among the VOCs, formaldehyde is

451   the largest radical contributor, but the radical production rate decreases by 9% on hazy

452   days, resulting from the reduction in luminous intensity. As described in Sect. 3.1,

453   acetaldehyde concentration is at a high level worldwide; therefore, its contribution to

454   radical production is significant and shows a 21% increase from non-hazy days to hazy

455   days. As acetone and propionaldehyde cannot be distinguished in the current method,

456   two radical production rates are listed assuming that only a single species exists.

457   Accordingly, the above two species have significantly different photolysis properties,

458   which results in some uncertainties in the calculations of the total radical production

459   rate and yield. Therefore, the radical yields are given as ranges indicating the probable

460   number of OH radicals generated when one carbonyl compound molecule is consumed

461   in the ambient air. During the investigated period, the yields are estimated to be within

462   0.38-0.43 under different conditions. The contribution of radicals from O_3 photolysis is

463   small in wintertime, and little difference is observed between non-hazy days and hazy

464   days.

465   Finally, the contributions of SOAFP and radical production among the resolved

466   source are demonstrated, which are calculated with the concentration of every VOC

467   species in each source and the relevant yields or photolysis rates. According to Fig. 6

468   (c), the top 2 contributors are solvent evaporation and industrial emission, followed by

469   residential heating and vehicle exhaust. Similarly, the averaged RO_X production rates

470   of each source are calculated with their resolved carbonyl concentrations and the

471   corresponding photolysis rates weighted by 16 non-hazy days' and 11 hazy days' values.

472   It should be explained that the photolysis rates of C3 carbonyls used in this section are

473   the average values of acetone and propionaldehyde. As shown in Fig. 6 (d), the potential

474   major sources of radical production are solvent evaporation, biogenic and secondary

475   production, industrial emissions, and vehicle exhaust.

476   **4. Conclusion**

477   VOCs are essential in SOA formation because of their dual roles as precursors and

478   oxidant producers. In this study, online measurements of NMVOCS are conducted for

479   the first time in urban Xinxiang, with some canister samples grabbed for supplemental

480   information. Overall, OVOCs are the category with the highest mixing ratio, which is

481   more than 5-fold higher than those of other categories. Herein, methanol, acetaldehyde

482   and C3 carbonyls are among the most abundant species. Benzenoids are the second

483   most abundant category, with benzene, toluene, and C8 aromatics as major components.

484   Secondary production is significant in this study, as the growth amount of OVOCs is

485   relatively larger than that of benzenoids on hazy days, which coincides with the source

486   analysis results. Compared with the other field studies in the world, the mixing ratio of

487   benzenoids such as benzene, toluene, C8 aromatics, as well as OVOCs including

488   acetaldehyde, and C3 carbonyls are at high levels, indicating intensive anthropogenic

489   emissions in Xinxiang. In total, six sources were resolved in this study, including

490   biogenic and secondary sources, solvent evaporation, residential heating, thermal

491   power generation, vehicle exhaust, and industrial emissions. Accordingly, benzenoids

492   are highly loaded with solvent evaporation, residential heating, and industrial emissions,

493   while the six resolved sources have similar contributions of total OVOCs. According

494   to the PSCF and CWT results, ambient VOCs are more likely influenced by local

495   emissions and short-distance transport. In brief, secondary products are transported

496   along with the air mass movement trajectory, while solvent evaporation and residential

497   heating sources are intense around the border cities in Henan and Shanxi Provinces. In

498   addition, thermal power generation, vehicle exhaust, and industrial emissions are

499   intensively released around the sampling site, with some hot spots in different directions.

500   Based on the SOAFP calculations, toluene and benzene are the top 2 SOA

501   contributors in the campaign, while the weights of their estimated production mass in

502   the observed SOA mass show a declining trend with the aggravation of pollution. On

503   the other hand, the OH exposure and SOA concentration exhibit a good relationship

504   throughout the observation period, which highlights the effect of atmospheric oxidation

505   capacity on SOA growth. From the estimation of the OH radical production rates,

506   formaldehyde is found to be the strongest radical contributor, while the contribution of

507   acetaldehyde is significant because of its high concentration in this study. Isomers such

508   as acetone and propionaldehyde cannot be distinguished in PTR-MS; therefore, the

509 radical production rate of C3 carbonyls is presented as a range. Because the photolysis

510 properties of the above isomers differ greatly, further analysis should be performed to

511 clarify the proportion of C3 carbonyls and their OH contributions. In this study, we

512 assigned SOAFP and radical production information into the resolved sources. The

513 results show that solvent evaporation is the dominant source for SOAFP and radical

514 production. Comparatively, residential heating has a greater impact on SOAFP, and

515 industrial emissions are more significant for radical production. Although traffic

516 restriction is conducted during the campaign, the influence of vehicle exhaust is still

517 non-neglectable in the two aspects. In addition, biogenic and secondary sources have

518 large potential in radical production, which could not be undervalued in autumn or even

519 in winter. This study provides first-hand information on VOC characteristics in a central

520 Chinese city and first evaluates the resolved sources with SOAFP and radical

521 production information. The results will provide targeted measures for SOA reduction.

522

523 *Data availability*. The observational data in this study are available from the authors

524 upon reasonable request (zhanghaixu@tsinghua.edu.cn).

525

526 *Author contributions.* HZ designed the experiments, carried out the field observation,

527 processed the data, and drafted the paper with contributions from all co-authors. CC

528 maintained the instruments during the campaign, processed ACSM data, and conducted

529 source apportionment analysis of organic aerosols. WY and NW assisted setting up

530 field campaigns and sampling. YB coordinated the field campaign. QZ and KH

531 supervised the project and revised the paper.

532

533 *Competing interests*. The authors declare that they have no conflict of interest.

534

535 *Acknowledgements.* This work was funded by the National Research Program for key

536 issues in air pollution control (DQGG0201) and National Natural Science Foundation

537 of China (41625020 and 41571130035). The authors would thank Xinxiang Ecological

538　Environmental Bureau for logistical support on the filed campaign.

539

540　**References**

541　An, J. L., Wang, Y. S., Wu, F. K., and Zhu, B.: Characterizations of volatile organic

542　　　compounds during high ozone episodes in Beijing, China, Environ. Monit. Assess.,

543　　　184, 1879-1889, 10.1007/s10661-011-2086-7, 2012.

544　Apel, E. C., Riemer, D. D., Hills, A., Baugh, W., Orlando, J., Faloona, I., Tan, D., Brune,

545　　　W., Lamb, B., Westberg, H., Carroll, M. A., Thornberry, T., and Geron, C. D.:

546　　　Measurement and interpretation of isoprene fluxes and isoprene, methacrolein,

547　　　and methyl vinyl ketone mixing ratios at the PROPHET site during the 1998

548　　　Intensive, J Geophys. Res.-Atmos., 107, 10.1029/2000jd000225, 2002.

549　Appel, K. W., Bhave, P. V., Gilliland, A. B., Sarwar, G., and Roselle, S. J.: Evaluation

550　　　of the community multiscale air quality (CMAQ) model version 4.5: Sensitivities

551　　　impacting model performance; Part II-particulate matter, Atmos. Environ., 42,

552　　　6057-6066, 10.1016/j.atmosenv.2008.03.036, 2008.

553　Atkinson, R., Arey, J., and Aschmann, S. M.: Atmospheric chemistry of alkanes:

554　　　Review and recent developments, Atmos. Environ., 42, 5859-5871,

555　　　https://doi.org/10.1016/j.atmosenv.2007.08.040, 2008.

556　Barletta, B., Meinardi, S., Sherwood Rowland, F., Chan, C. Y., Wang, X., Zou, S., Yin

557　　　Chan, L., and Blake, D. R.: Volatile organic compounds in 43 Chinese cities,

558　　　Atmos. Environ., 39, 5979-5990, https://doi.org/10.1016/j.atmosenv.2005.06.029,

559　　　2005.

560　Brito, J., Wurm, F., Yanez-Serrano, A. M., de Assuncao, J. V., Godoy, J. M., and Artaxo,

561　　　P.: Vehicular Emission Ratios of VOCs in a Megacity Impacted by Extensive

562　　　Ethanol Use: Results of Ambient Measurements in Sao Paulo, Brazil, Environ. Sci.

563　　　Technol., 49, 11381-11387, 10.1021/acs.est.5b03281, 2015.

564　Calvert, J. G. A., Roger; Becker, Karl H.; Kamens, Richard M.; Seinfeld, John H.;

565　　　Wallington, Timothy J.; Yarwood, Greg: The Mechanisms of Atmospheric

566　　　Oxidation of Aromatic Hydrocarbons (Eds.), Oxford University Press, New York,

567　　　556, 2002.

Atmospheric
Chemistry
and Physics
Discussions
Open Access
EGU

568   Chen, W. T., Shao, M., Lu, S. H., Wang, M., Zeng, L. M., Yuan, B., and Liu, Y.:

569   Understanding primary and secondary sources of ambient carbonyl compounds in

570   Beijing using the PMF model, Atmos. Chem. Phys., 14, 3047-3062, 10.5194/acp-

571   14-3047-2014, 2014.

572   Chen, Z. H., Cheng, S. Y., Li, J. B., Guo, X. R., Wang, W. H., and Chen, D. S.:

573   Relationship between atmospheric pollution processes and synoptic pressure

574   patterns   in   northern   China,   Atmos.   Environ.,   42,   6078-6087,

575   https://doi.org/10.1016/j.atmosenv.2008.03.043, 2008.

576   Crounse, J. D., Nielsen, L. B., Jorgensen, S., Kjaergaard, H. G., and Wennberg, P. O.:

577   Autoxidation of Organic Compounds in the Atmosphere, J Phys. Chem. Lett., 4,

578   3513-3520, 10.1021/jz4019207, 2013.

579   Crutzen, P. J., and Zimmermann, P. H.: The changing photochemistry of the troposphere,

580   Tellus, 43, 136-151, 1991.

581   de Gouw, J. A., Middlebrook, A. M., Warneke, C., Goldan, P. D., Kuster, W. C., Roberts,

582   J. M., Fehsenfeld, F. C., Worsnop, D. R., Canagaratna, M. R., Pszenny, A. A. P.,

583   Keene, W. C., Marchewka, M., Bertman, S. B., and Bates, T. S.: Budget of organic

584   carbon in a polluted atmosphere: Results from the New England Air Quality Study

585   in 2002, J Geophys. Res.-Atmos., 110, 10.1029/2004jd005623, 2005.

586   Ding, X., He, Q. F., Shen, R. Q., Yu, Q. Q., and Wang, X.-M.: Spatial distributions of

587   secondary organic aerosols from isoprene, monoterpenes, beta-caryophyllene, and

588   aromatics over China during summer, J Geophys. Res.Atmos., 119, 11877-11891,

589   10.1002/2014jd021748, 2014.

590   Duan, J., Guo, S., Tan, J., Wang, S., and Chai, F.: Characteristics of atmospheric

591   carbonyls   during   haze   days   in   Beijing,   China,   Atmos.   Res.,   114,   17-27,

592   10.1016/j.atmosres.2012.05.010, 2012.

593   Edwards, P. M., Brown, S. S., Roberts, J. M., Ahmadov, R., Banta, R. M., deGouw, J.

594   A., Dubé, W. P., Field, R. A., Flynn, J. H., Gilman, J. B., Graus, M., Helmig, D.,

595   Koss, A., Langford, A. O., Lefer, B. L., Lerner, B. M., Li, R., Li, S. M., McKeen,

596   S. A., Murphy, S. M., Parrish, D. D., Senff, C. J., Soltis, J., Stutz, J., Sweeney, C.,

597   Thompson, C. R., Trainer, M. K., Tsai, C., Veres, P. R., Washenfelder, R. A.,
598   Warneke, C., Wild, R. J., Young, C. J., Yuan, B., and Zamora, R.: High winter
599   ozone pollution from carbonyl photolysis in an oil and gas basin, Nature, 514, 351,
600   10.1038/nature13767, 2014.

601   Ehhalt, D. H., and Rohrer, F.: Dependence of the OH concentration on solar UV, J
602   Geophys. Res.-Atmos., 105, 3565-3571, 10.1029/1999jd901070, 2000.

603   Emmerson, K. M., Carslaw, N., and Pilling, M. J.: Urban atmospheric chemistry during
604   the PUMA campaign 2: Radical budgets for OH, HO_2 and RO_2, J Atmos. Chem.,
605   52, 165-183, 10.1007/s10874-005-1323-2, 2005.

606   EPA, U.: Compendium Method TO-15: Determination of volatile organic compounds
607   in air collected in specially prepared canisters and analysed by gas
608   chromatography/mass spectrometry, 1999. Available:
609   http://www.epa.gov/ttnamti1/files/ambien? t/airtox/to-15r.pdf. Accessed 2012.

610   Gao, Y., Wang, H., Zhang, X., Jing, S. a., Peng, Y., Qiao, L., Zhou, M., Huang, D. D.,
611   Wang, Q., Li, X., Li, L., Feng, J., Ma, Y., and Li, Y.: Estimating Secondary Organic
612   Aerosol Production from Toluene Photochemistry in a Megacity of China, Environ.
613   Sci. Technol., 53, 8664-8671, 10.1021/acs.est.9b00651, 2019.

614   Greene, J. S., Kalkstein, L. S., Ye, H., and Smoyer, K.: Relationships between synoptic
615   climatology and atmospheric pollution at 4 US cities, Theor. Appl. Climatol., 62,
616   163-174, 10.1007/s007040050081, 1999.

617   Grosjean, D., and Seinfeld, J. H.: Parameterization of the formation potential of
618   secondary organic aerosols, Atmos. Environ., 23, 1733-1747, 10.1016/0004-
619   6981(89)90058-9, 1989.

620   Guo, S., Hu, M., Zamora, M. L., Peng, J., Shang, D., Zheng, J., Du, Z., Wu, Z., Shao,
621   M., Zeng, L., Molina, M. J., and Zhang, R.: Elucidating severe urban haze
622   formation in China, P Natl. Acad. Sci. US, 111, 17373-17378,
623   10.1073/pnas.1419604111, 2014.

624   Han, S., Zhao, Q., Zhang, R., Liu, Y., Li, C., Zhang, Y., Li, Y., Yin, S., and Yan, Q.:
625   Emission characteristic and environmental impact of process-based VOCs from

Atmospheric
Chemistry
and Physics
Discussions
Open Access
EGU

626   prebaked anode manufacturing industry in Zhengzhou, China, Atmos. Pollut. Res.,

627   11, 67-77, 10.1016/j.apr.2019.09.016, 2020.

628 Holzinger, R., Williams, J., Salisbury, G., Klüpfel, T., de Reus, M., Traub, M., Crutzen,

629   P. J., and Lelieveld, J.: Oxygenated compounds in aged biomass burning plumes

630   over the Eastern Mediterranean: evidence for strong secondary production of

631   methanol and acetone, Atmos. Chem. Phys., 5, 39-46, 10.5194/acp-5-39-2005,

632   2005.

633 Huang, R.J., Zhang, Y., Bozzetti, C., Ho, K.F., Cao, J.J., Han, Y., Daellenbach, K. R.,

634   Slowik, J. G., Platt, S. M., Canonaco, F., Zotter, P., Wolf, R., Pieber, S. M., Bruns,

635   E. A., Crippa, M., Ciarelli, G., Piazzalunga, A., Schwikowski, M., Abbaszade, G.,

636   Schnelle-Kreis, J., Zimmermann, R., An, Z., Szidat, S., Baltensperger, U., El

637   Haddad, I., and Prevot, A. S. H.: High secondary aerosol contribution to particulate

638   pollution during haze events in China, Nature, 514, 218-222, 10.1038/nature13774,

639   2014.

640 Huang, X.F., Wang, C., Zhu, B., Lin, L.L., and He, L.Y.: Exploration of sources of

641   OVOCs in various atmospheres in southern China, Environ. Pollut., 249, 831-842,

642   https://doi.org/10.1016/j.envpol.2019.03.106, 2019.

643 Jathar, S. H., Mahmud, A., Barsanti, K. C., Asher, W. E., Pankow, J. F., and Kleeman,

644   M. J.: Water uptake by organic aerosol and its influence on gas/particle partitioning

645   of secondary organic aerosol in the United States, Atmos. Environ., 129, 142-154,

646   https://doi.org/10.1016/j.atmosenv.2016.01.001, 2016.

647 Kristensson, A., Johansson, C., Westerholm, R., Swietlicki, E., Gidhagen, L., Wideqvist,

648   U., and Vesely, V.: Real-world traffic emission factors of gases and particles

649   measured in a road tunnel in Stockholm, Sweden, Atmos. Environ., 38, 657-673,

650   10.1016/j.atmosenv.2003.10.030, 2004.

651 Kroll, J. H., and Seinfeld, J. H.: Chemistry of secondary organic aerosol: Formation and

652   evolution of low-volatility organics in the atmosphere, Atmos. Environ., 42, 3593-

653   3624, https://doi.org/10.1016/j.atmosenv.2008.01.003, 2008.

654 Lelieveld, J., Butler, T. M., Crowley, J. N., Dillon, T. J., Fischer, H., Ganzeveld, L.,

655   Harder, H., Lawrence, M. G., Martinez, M., Taraborrelli, D., and Williams, J.:

656   Atmospheric oxidation capacity sustained by a tropical forest, Nature, 452, 737-

657   740, 10.1038/nature06870, 2008.

658   Li, B., Ho, S. S. H., Gong, S., Ni, J., Li, H., Han, L., Yang, Y., Qi, Y., and Zhao, D.:

659   Characterization of VOCs and their related atmospheric processes in a central

660   Chinese city during severe ozone pollution periods, Atmos. Chem. Phys., 19, 617-

661   638, 10.5194/acp-19-617-2019, 2019a.

662   Li, H., Zhang, Q., Zheng, B., Chen, C., Wu, N., Guo, H., Zhang, Y., Zheng, Y., Li, X.,

663   and He, K.: Nitrate-driven urban haze pollution during summertime over the North

664   China Plain, Atmos. Chem. Phys., 18, 5293-5306, 10.5194/acp-18-5293-2018,

665   2018.

666   Li, J., Cleveland, M., Ziemba, L. D., Griffin, R. J., Barsanti, K. C., Pankow, J. F., and

667   Ying, Q.: Modeling regional secondary organic aerosol using the Master Chemical

668   Mechanism, Atmos. Environ., 102, 52-61, 10.1016/j.atmosenv.2014.11.054, 2015.

669   Li, K., Li, J., Tong, S., Wang, W., Huang, R.-J., and Ge, M.: Characteristics of

670   wintertime VOCs in suburban and urban Beijing: concentrations, emission ratios,

671   and festival effects, Atmos. Chem. Phys., 19, 8021-8036, 10.5194/acp-19-8021-

672   2019, 2019b.

673   Li, Y., Shao, M., Lu, S., Chang, C. C., and Dasgupta, P. K.: Variations and sources of

674   ambient formaldehyde for the 2008 Beijing Olympic games, Atmos. Environ., 44,

675   2632-2639, https://doi.org/10.1016/j.atmosenv.2010.03.045, 2010.

676   Liang, H., Chen, Z. M., Huang, D., Zhao, Y., and Li, Z. Y.: Impacts of aerosols on the

677   chemistry of atmospheric trace gases: a case study of peroxides and HO_2 radicals,

678   Atmos. Chem. Phys., 13, 11259-11276, 10.5194/acp-13-11259-2013, 2013.

679   Lim, Y. B., and Ziemann, P. J.: Effects of Molecular Structure on Aerosol Yields from

680   OH Radical-Initiated Reactions of Linear, Branched, and Cyclic Alkanes in the

681   Presence of NOx, Environ. Sci. Technol., 43, 2328-2334, 10.1021/es803389s,

682   2009.

683   Lindinger, W., Hansel, A., and Jordan, A.: On-line monitoring of volatile organic

Atmospheric
Chemistry
and Physics
Discussions

684   compounds at pptv levels by means of proton-transfer-reaction mass spectrometry

685   (PTR-MS) - Medical applications, food control and environmental research, Int. J

686   Mass Spectrom., 173, 191-241, 10.1016/s0168-1176(97)00281-4, 1998.

687   Liu, C., Z. Ma, Y. Mu, J. Liu, C. Zhang, Y. Zhang, P. Liu, and H. Zhang (2017), The

688   levels, variation characteristics, and sources of atmospheric non-methane

689   hydrocarbon compounds during wintertime in Beijing, China, Atmos. Chem.

690   Phys., 17(17), 10633-10649, doi:10.5194/acp-17-10633-2017.

691   Liu, K. K., Zhang, C. L., Cheng, Y., Liu, C. T., Zhang, H. X., Zhang, G., Sun, X., and

692   Mu, Y. J.: Serious BTEX pollution in rural area of the North China Plain during

693   winter season, J Environ. Sci., 30, 186-190, 10.1016/j.jes.2014.05.056, 2015.

694   Liu, Z., Wang, Y., Gu, D., Zhao, C., Huey, L. G., Stickel, R., Liao, J., Shao, M., Zhu,

695   T., Zeng, L., Amoroso, A., Costabile, F., Chang, C. C., and Liu, S. C.: Summertime

696   photochemistry during CAREBeijing-2007: RO_x budgets and O_3 formation,

697   Atmos. Chem. Phys., 12, 7737-7752, 10.5194/acp-12-7737-2012, 2012.

698   Ng, N. L., Kroll, J. H., Chan, A. W. H., Chhabra, P. S., Flagan, R. C., and Seinfeld, J.

699   H.: Secondary organic aerosol formation from m-xylene, toluene, and benzene,

700   Atmos. Chem. Phys., 7, 3909-3922, 10.5194/acp-7-3909-2007, 2007.

701   Ng, N. L., Herndon, S. C., Trimborn, A., Canagaratna, M. R., Croteau, P. L., Onasch, T.

702   B., Sueper, D., Worsnop, D. R., Zhang, Q., Sun, Y. L., and Jayne, J. T.: An Aerosol

703   Chemical Speciation Monitor (ACSM) for Routine Monitoring of the

704   Composition and Mass Concentrations of Ambient Aerosol, Aerosol Sci. Tech., 45,

705   780-794, 10.1080/02786826.2011.560211, 2011.

706   Norris G., R. D. S. B., AND S. Bai: EPA Positive Matrix Factorization (PMF) 5.0

707   Fundamentals and User Guide, in, edited by: Agency, U. S. E. P., Washington, DC,

708   2014.

709   Odum, J. R., Hoffmann, T., Bowman, F., Collins, D., Flagan, R. C., and Seinfeld, J. H.:

710   Gas/particle partitioning and secondary organic aerosol yields, Environ. Sci.

711   Technol., 30, 2580-2585, 10.1021/es950943+, 1996.

712   Qi, X., Hao, Q. J., Ji, D. S., Zhang, J. S., Liu, Z. R., Ru, B., Wang, Y. S., and Jiang, C.

713   S.: Composition Characteristics of Atmospheric Volatile Organic Compounds in

714   the Urban Area of Beibei District, Chongqing, Huanjing Kexue, 35, 3293-3301,

715   2014.

716   Qian, X., Shen, H. Q., and Chen, Z. M.: Characterizing summer and winter carbonyl

717   compounds in Beijing atmosphere, Atmos. Environ., 214, 10,

718   10.1016/j.atmosenv.2019.116845, 2019.

719   Rao, Z., Chen, Z., Liang, H., Huang, L., and Huang, D.: Carbonyl compounds over

720   urban Beijing: Concentrations on haze and non-haze days and effects on radical

721   chemistry, Atmos. Environ., 124, 207-216, 10.1016/j.atmosenv.2015.06.050, 2016.

722   Rollins, A. W., Browne, E. C., Min, K. E., Pusede, S. E., Wooldridge, P. J., Gentner, D.

723   R., Goldstein, A. H., Liu, S., Day, D. A., Russell, L. M., and Cohen, R. C.:

724   Evidence for NOx control over nighttime SOA formation, Science, 337, 1210-

725   1212, 10.1126/science.1221520, 2012.

726   Sahu, L. K., and Saxena, P.: High time and mass resolved PTR-TOF-MS measurements

727   of VOCs at an urban site of India during winter: Role of anthropogenic, biomass

728   burning, biogenic and photochemical sources, Atmos. Res., 164-165, 84-94,

729   https://doi.org/10.1016/j.atmosres.2015.04.021, 2015.

730   Sahu, L. K., Yadav, R., and Pal, D.: Source identification of VOCs at an urban site of

731   western India: Effect of marathon events and anthropogenic emissions, J Geophys.

732   Res.-Atmos.,121, 2416-2433, 10.1002/2015jd024454, 2016.

733   Santos, F., Longo, K., Guenther, A., Kim, S., Gu, D., Oram, D., Forster, G., Lee, J.,

734   Hopkins, J., Brito, J., and Freitas, S.: Biomass burning emission disturbances of

735   isoprene oxidation in a tropical forest, Atmos. Chem. Phys., 18, 12715-12734,

736   10.5194/acp-18-12715-2018, 2018.

737   Sarkar, C., Sinha, V., Sinha, B., Panday, A. K., Rupakheti, M., and Lawrence, M. G.:

738   Source apportionment of NMVOCs in the Kathmandu Valley during the SusKat-

739   ABC international field campaign using positive matrix factorization, Atmos.

740   Chem. Phys., 17, 8129-8156, 10.5194/acp-17-8129-2017, 2017.

741   Sarrafzadeh, M., Wildt, J., Pullinen, I., Springer, M., Kleist, E., Tillmann, R., Schmitt,

742   S. H., Wu, C., Mentel, T. F., Zhao, D., Hastie, D. R., and Kiendler-Scharr, A.:

743   Impact of NOx and OH on secondary organic aerosol formation from beta-pinene

744   photooxidation, Atmos. Chem. Phys., 16, 11237-11248, 10.5194/acp-16-11237-

745   2016, 2016.

746   Shao, M., Wang, B., Lu, S., Yuan, B., and Wang, M.: Effects of Beijing Olympics

747   Control Measures on Reducing Reactive Hydrocarbon Species, Environ. Sci.

748   Technol., 45, 514-519, 10.1021/es102357t, 2011.

749   Sheng, J. J., Zhao, D. L., Ding, D. P., Li, X., Huang, M. Y., Gao, Y., Quan, J. N., and

750   Zhang, Q.: Characterizing the level, photochemical reactivity, emission, and

751   source contribution of the volatile organic compounds based on PTR-TOF-MS

752   during winter haze period in Beijing, China, Atmos. Res., 212, 54-63,

753   10.1016/j.atmosres.2018.05.005, 2018.

754   Singh, H. B., O'Hara, D., Herlth, D., Sachse, W., Blake, D. R., Bradshaw, J. D.,

755   Kanakidou, M., and Crutzen, P. J.: Acetone in the atmosphere: Distribution,

756   sources, and sinks, J Geophys. Res.-Atmos., 99, 1805-1819, 10.1029/93jd00764,

757   1994.

758   Sinha, V., Kumar, V., and Sarkar, C.: Chemical composition of pre-monsoon air in the

759   Indo-Gangetic Plain measured using a new air quality facility and PTR-MS: high

760   surface ozone and strong influence of biomass burning, Atmos. Chem. Phys., 14,

761   5921-5941, 10.5194/acp-14-5921-2014, 2014.

762   Stroud, C. A., Roberts, J. M., Goldan, P. D., Kuster, W. C., Murphy, P. C., Williams, E.

763   J., Hereid, D., Parrish, D., Sueper, D., Trainer, M., Fehsenfeld, F. C., Apel, E. C.,

764   Riemer, D., Wert, B., Henry, B., Fried, A., Martinez-Harder, M., Harder, H., Brune,

765   W. H., Li, G., Xie, H., and Young, V. L.: Isoprene and its oxidation products,

766   methacrolein and methylvinyl ketone, at an urban forested site during the 1999

767   Southern   Oxidants   Study,   J   Geophys.   Res.-Atmos.,   106,   8035-8046,

768   10.1029/2000jd900628, 2001.

769   Su, W., Liu, C., Hu, Q., Zhao, S., Sun, Y., Wang, W., Zhu, Y., Liu, J., and Kim, J.:

770   Primary and secondary sources of ambient formaldehyde in the Yangtze River

771   Delta based on Ozone Mapping and Profiler Suite (OMPS) observations, Atmos.

772   Chem. Phys., 19, 6717-6736, 10.5194/acp-19-6717-2019, 2019.

773 Sun, Y., Wang, Z., Fu, P., Jiang, Q., Yang, T., Li, J., and Ge, X.: The impact of relative

774   humidity on aerosol composition and evolution processes during wintertime in

775   Beijing,   China,   Atmos.   Environ.,   77,   927-934,

776   https://doi.org/10.1016/j.atmosenv.2013.06.019, 2013.

777 Tang, R., Wu, Z., Li, X., Wang, Y., Shang, D., Xiao, Y., Li, M., Zeng, L., Wu, Z.,

778   Hallquist, M., Hu, M., and Guo, S.: Primary and secondary organic aerosols in

779   summer 2016 in Beijing, Atmos. Chem. Phys., 18, 4055-4068, 10.5194/acp-18-

780   4055-2018, 2018.

781 Tsimpidi, A. P., Karydis, V. A., Zavala, M., Lei, W., Bei, N., Molina, L., and Pandis, S.

782   N.: Sources and production of organic aerosol in Mexico City: insights from the

783   combination of a chemical transport model (PMCAMx-2008) and measurements

784   during MILAGRO, Atmos. Chem. Phys., 11, 5153-5168, 10.5194/acp-11-5153-

785   2011, 2011.

786 Wang, C., Huang, X. F., Han, Y., Zhu, B., and He, L. Y.: Sources and potential

787   photochemical roles of formaldehyde in an urban atmosphere in south China, J

788   Geophys. Res.-Atmos., 122, 11,934-911,947, 10.1002/2017jd027266, 2017.

789 Warneke, C., McKeen, S. A., de Gouw, J. A., Goldan, P. D., Kuster, W. C., Holloway,

790   J. S., Williams, E. J., Lerner, B. M., Parrish, D. D., Trainer, M., Fehsenfeld, F. C.,

791   Kato, S., Atlas, E. L., Baker, A., and Blake, D. R.: Determination of urban volatile

792   organic compound emission ratios and comparison with an emissions database, J

793   Geophys. Res.,112, 10.1029/2006jd007930, 2007.

794 Wu, R., and Xie, S.: Spatial distribution of secondary organic aerosol formation

795   potential in china derived from speciated anthropogenic volatile organic

796   compound   emissions,   Environ.   Sci.   Technol.,   52,   8146-8156,

797   10.1021/acs.est.8b01269, 2018.

798 Wu, W., Zhao, B., Wang, S., and Hao, J.: Ozone and secondary organic aerosol

799   formation potential from anthropogenic volatile organic compounds emissions in

800   China, J Environ. Sci., 53, 224-237, 10.1016/j.jes.2016.03.025, 2017.

801 Xing, L., Wu, J., Elser, M., Tong, S., Liu, S., Li, X., Liu, L., Cao, J., Zhou, J., El-Haddad,

802   I., Huang, R., Ge, M., Tie, X., Prevot, A. S. H., and Li, G.: Wintertime secondary

803   organic aerosol formation in Beijing-Tianjin-Hebei (BTH): contributions of

804   HONO sources and heterogeneous reactions, Atmos. Chem. Phys., 19, 2343-2359,

805   10.5194/acp-19-2343-2019, 2019.

806 Yang, H., Zhu, B., Gao, J.-h., Li, Y.-y., and Xia, L.: Source apportionment of VOCs in

807   the northern suburb of Nanjing in summer, Huanjing Kexue, 34, 4519-4528, 2013.

808 Yang, X., Xue, L., Yao, L., Li, Q., Wen, L., Zhu, Y., Chen, T., Wang, X., Yang, L., Wang,

809   T., Lee, S., Chen, J., and Wang, W.: Carbonyl compounds at Mount Tai in the North

810   China Plain: Characteristics, sources, and effects on ozone formation, Atmos. Res.,

811   196, 53-61, 10.1016/j.atmosres.2017.06.005, 2017.

812 Yang, Z., Cheng, H. R., Wang, Z. W., Peng, J., Zhu, J. X., Lyu, X. P., and Guo, H.:

813   Chemical characteristics of atmospheric carbonyl compounds and source

814   identification of formaldehyde in Wuhan, Central China, Atmos. Res., 228, 95-

815   106, 10.1016/j.atmosres.2019.05.020, 2019.

816 Yuan, B., Hu, W. W., Shao, M., Wang, M., Chen, W. T., Lu, S. H., Zeng, L. M., and Hu,

817   M.: VOC emissions, evolutions and contributions to SOA formation at a receptor

818   site in eastern China, Atmos. Chem. Phys., 13, 8815-8832, 10.5194/acp-13-8815-

819   2013, 2013.

820 Zhang, J., Zhao, Y., Zhao, Q., Shen, G., Liu, Q., Li, C., Zhou, D., and Wang, S.:

821   Characteristics and source apportionment of summertime volatile organic

822   compounds in a fast developing city in the Yangtze River Delta, China,

823   Atmosphere, 9, 10.3390/atmos9100373, 2018.

824 Zhang, X., Cappa, C. D., Jathar, S. H., McVay, R. C., Ensberg, J. J., Kleeman, M. J.,

825   and Seinfeld, J. H.: Influence of vapor wall loss in laboratory chambers on yields

826   of secondary organic aerosol, P Natl. Acad. Sci. US., 111, 5802-5807,

827   10.1073/pnas.1404727111, 2014.

828 Zhang, X., Xue, Z., Li, H., Yan, L., Yang, Y., Wang, Y., Duan, J., Li, L., Chai, F., Cheng,

829   M., and Zhang, W.: Ambient volatile organic compounds pollution in China, J
830   Environ. Sci., 55, 69-75, 10.1016/j.jes.2016.05.036, 2017.
831 Zhang, Z., Wang, X., Zhang, Y., Lü, S., Huang, Z., Huang, X., and Wang, Y.: Ambient
832   air benzene at background sites in China's most developed coastal regions:
833   Exposure levels, source implications and health risks, Science of The Total
834   Environment, 511, 792-800, https://doi.org/10.1016/j.scitotenv.2015.01.003, 2015.
835 Zheng, H., Kong, S., Xing, X., Mao, Y., Hu, T., Ding, Y., Li, G., Liu, D., Li, S., and Qi,
836   S.: Monitoring of volatile organic compounds (VOCs) from an oil and gas station
837   in northwest China for 1 year, Atmos. Chem. Phys., 18, 4567-4595, 10.5194/acp-
838   18-4567-2018, 2018.
839 Zheng, J., Zhang, R., Garzón, J. P., Huertas, M. E., Levy, M., Ma, Y., Torres-Jardón, R.,
840   Ruiz-Suárez, L. G., Russell, L., Takahama, S., Tan, H., Li, G., and Molina, L. T.:
841   Measurements of formaldehyde at the U.S.–Mexico border during the Cal-Mex
842   2010 air quality study, Atmos. Environ., 70, 513-520,
843   https://doi.org/10.1016/j.atmosenv.2012.09.041, 2013.
844

845

846

847

848
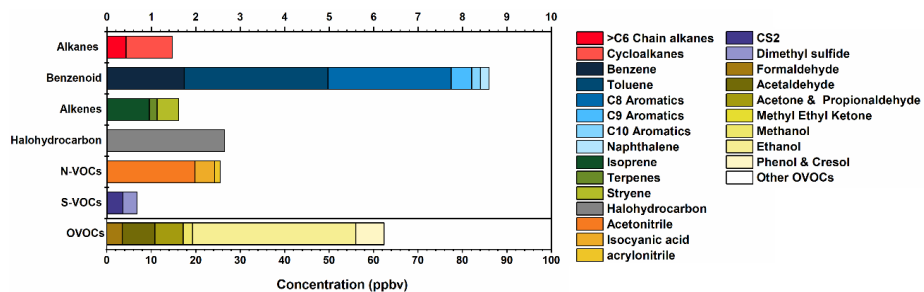
849 Figure 1. The average concentrations of VOCs observed in Xinxiang.

850
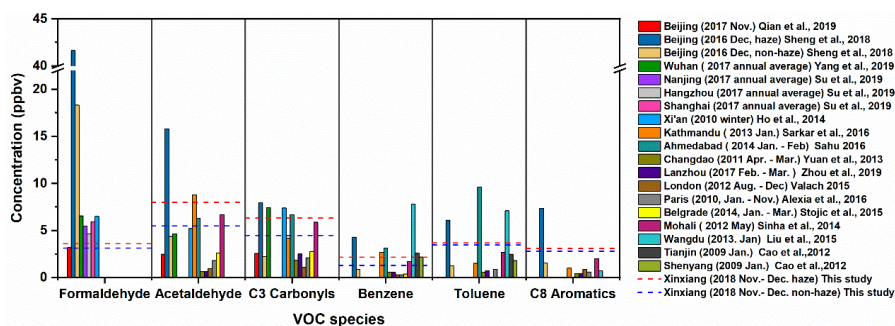
851

852　Figure 2. Comparison of average concentrations of OVOC and benzenoids in Xinxiang

853　Valley (hazy and non-hazy periods) with VOC levels at other sites worldwide.

854

855
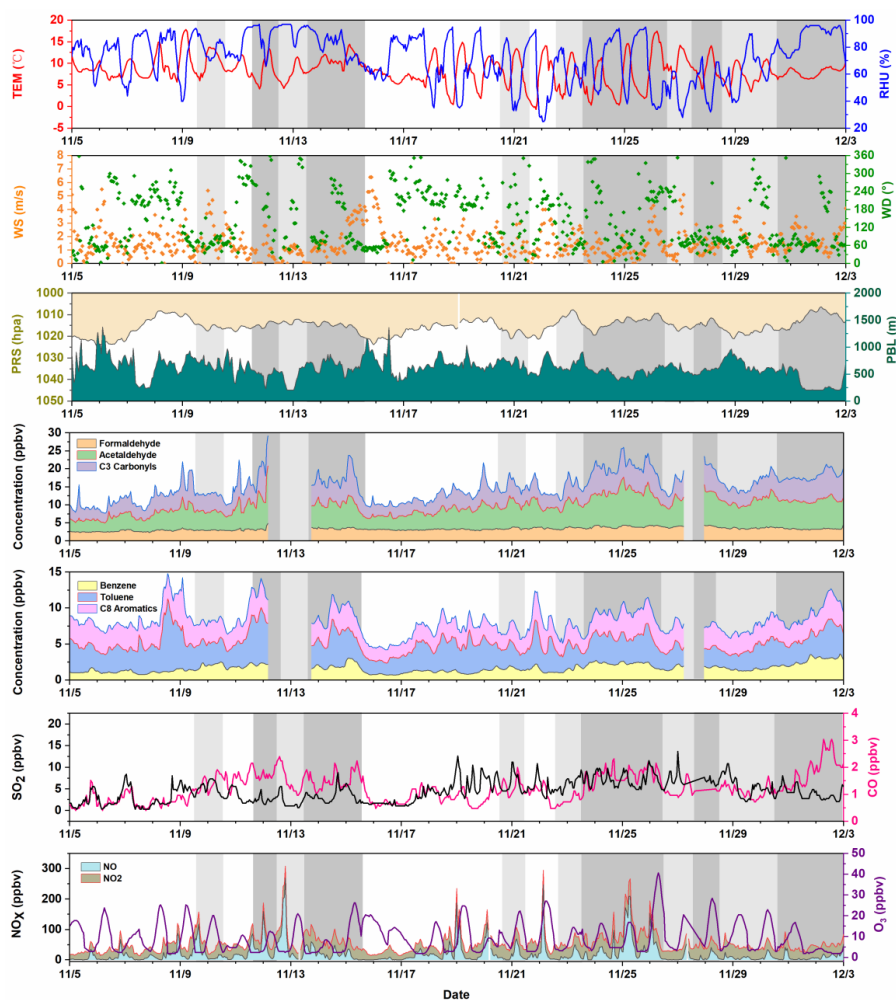
Figure 3. Time series of meteorological parameters and pollutant concentrations in
Xinxiang during the sampling period. The colours of the background represent the daily
averaged concentration levels of $PM_{2.5}$, and white, light grey, and dark grey represent
0-75 μg m^{-3}, 75-115 μg m^{-3}, and >115 μg m^{-3}, respectively.

861
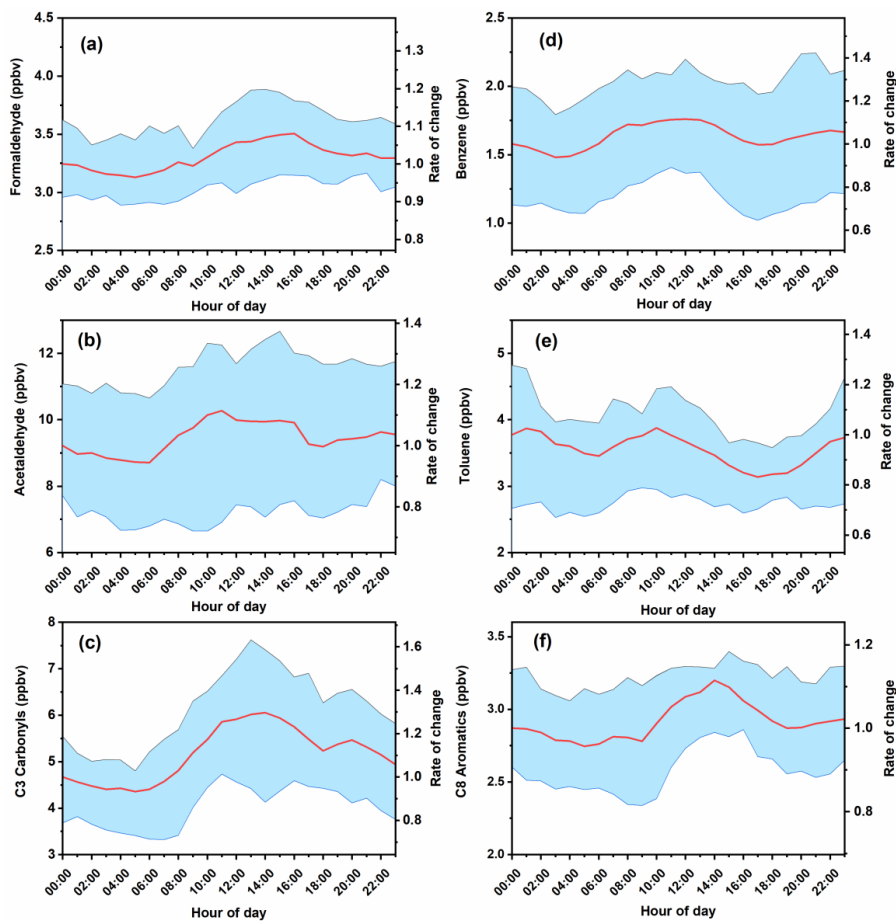
Figure 4. Diurnal variations of formaldehyde (a), acetaldehyde (b), C3 carbonyls (c), benzene (d), toluene (e), and C8 aromatics (f).

866
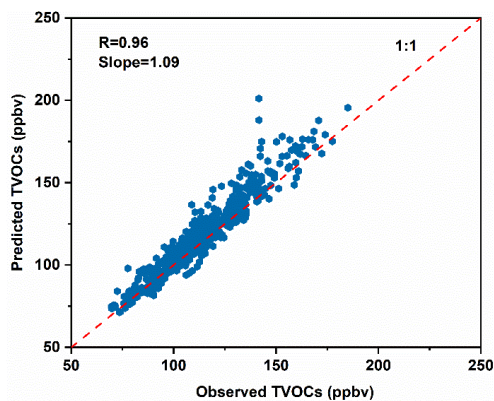
Figure 5. Correlation between observed and estimated VOC concentrations from the
PMF model.

869
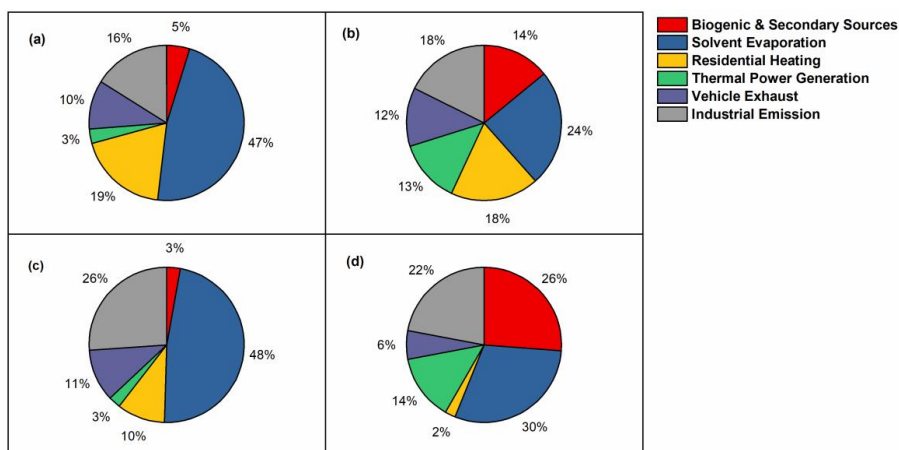
Figure 6. The contributions of different sources derived from the PMF model to benzenoids (a), carbonyl compounds (b), SOAFP (c), and radical generation rate (d).
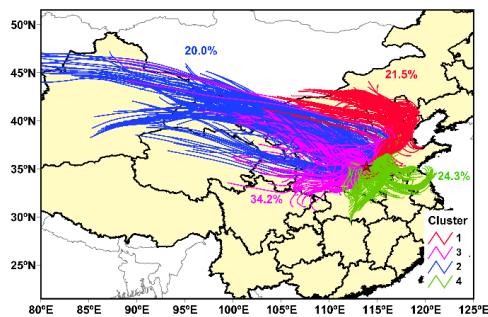
874

875 Figure 7. Cluster analysis of 48 h backward trajectories for Xinxiang from 2018.11.05
876 to 2018.12.03, with the percentage of each cluster presented.

877

878

879

880
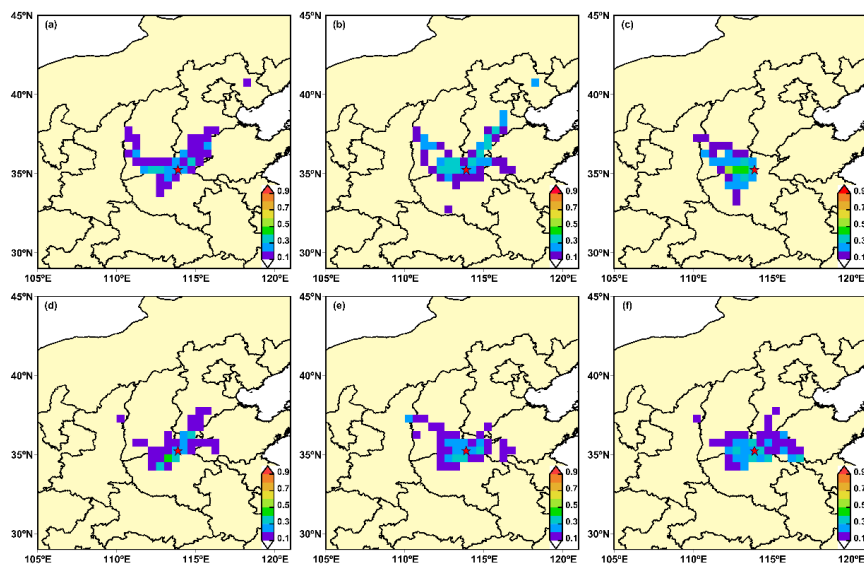
Figure 8. Weight potential source contribution function (WPSCF) maps for identified sources derived from PMF analysis including biogenic and secondary sources (a), solvent evaporation (b), residential heating (c), thermal power generation (d), vehicle exhaust (e), and industrial emissions (f).

885
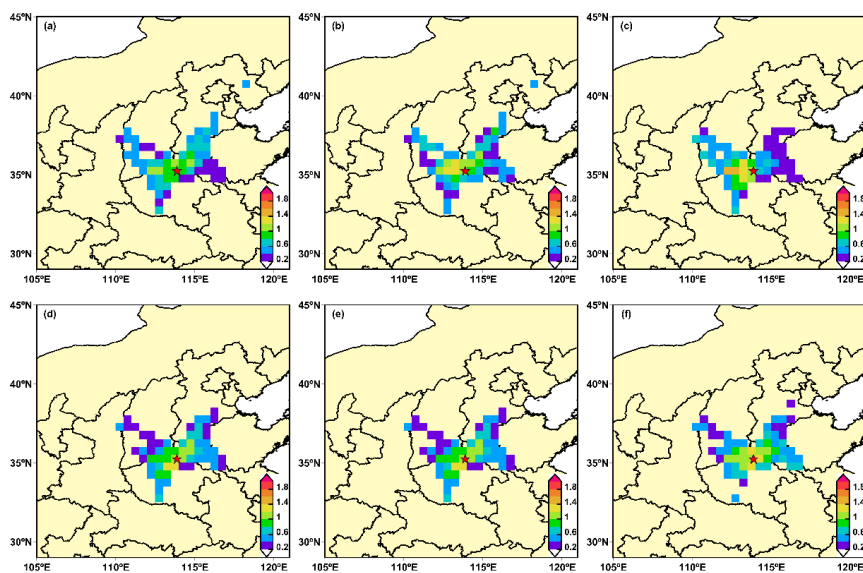
Figure 9. Weight concentration-weighted trajectory (WCWT) maps for identified sources derived from PMF analysis including biogenic and secondary sources (a), solvent evaporation (b), residential heating (c), thermal power generation (d), vehicle exhaust (e), and industrial emissions (f).

Atmospheric
Chemistry
and Physics
Discussions

Open Access

EGU
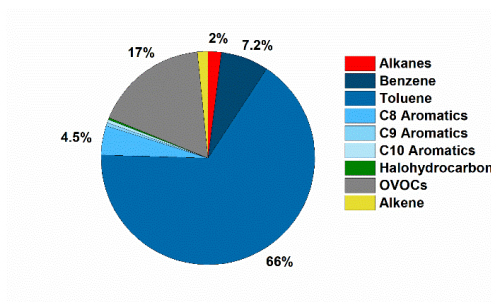
892

893   Figure 10. Chemical distribution of SOAFP during the sampling period in Xinxiang.

894

895
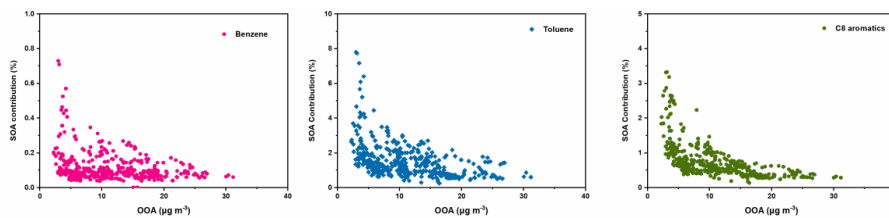
896

897 Fig. 11 SOA contributions generated by benzene (a), toluene (b), and C8 aromatics (c)
898 with increasing OOA concentration.

899

900 **Table 1. The modelled daytime (8:00-16:00 LT) average OH concentration ($\times 10^6$ molec cm^{-3})**
901 **and radical production rate (P, $\times 10^6$ molec cm^{-3} s^{-1}) of O$_3$ and carbonyls and OH radical yield**
902 **(Y) from photolysis of carbonyl compounds.**
903

	OH concentration	P_{O_3}	P_{HCHO}	P_{CH_3CHO}	$P_{C_2H_5CHO}$	$P_{(CH_3)_2CHO}$	Y
Non-hazy days	0.62	0.07	1.31	0.24	0.85	0.01	0.39-0.43
Hazy days	0.46	0.07	1.19	0.29	0.95	0.01	0.38-0.40

904
905
906